Size of the smallest particles in Saturn's rings

Ohtsuki, Keiji
Kawamura, Hiroshi
Hirata, Naoyuki
Daisaka, Hiroshi
Kimura, Hiroshi

Draft version June 11, 2019
Typeset using LaTeX **manuscript** style in AASTeX62

Size of the Smallest Particles in Saturn's Rings

Keiji Ohtsuki,[1] Hiroshi Kawamura,[1] Naoyuki Hirata,[1] Hiroshi Daisaka,[2] and Hiroshi Kimura[3]

[1] *Department of Planetology, Kobe University, Kobe, 657-8501, Japan*

[2] *Graduate School of Commerce and Management, Hitotsubashi University, Tokyo 186-8601, Japan*

[3] *Planetary Exploration Research Center, Chiba Institute of Technology, Narashino 275-0016, Japan*

(Received January 13, 2019; Revised May 2, 2019; Accepted June 10, 2019)

Submitted to Icarus

ABSTRACT

Spacecraft and ground-based observations have shown that particles in Saturn's main rings have a power-law distribution roughly between centimeter and ten meters, but sub-centimeter particles appear to be lacking. Recent studies based on Cassini observations suggest that the minimum particle size is on the order of millimeters, although their abundance is lower than is expected from the extrapolation of the power-law distribution for the larger size range. Cohesive force between particles has been proposed to explain the paucity of sub-centimeter particles, but its strength depends on impact velocity. In order to better understand recent Cassini observations about small ring particles, we examine impact velocity ($v_{\rm imp}$) between ring particles using N-body simulation including size distribution. We find that most collisions take place at low velocities with $v_{\rm imp} \lesssim$

Corresponding author: Keiji Ohtsuki
ohtsuki@tiger.kobe-u.ac.jp

0.1 cm s^{-1}; even in dense rings where particles' velocity dispersion is enhanced by gravitational wakes, they collide at such low velocities because particles tend to move coherently in the wakes. This velocity is too low to detach sub-centimeter particles that are attached to the surface of large ones due to the cohesive force, explaining their paucity in the main rings. On the other hand, impacts at higher velocities occasionally occur, either as collision between particles in the high-velocity tail in dilute rings, or as collisions between adjacent wakes in the case of dense rings. Such infrequent high-velocity impacts release millimeter-sized particles strongly attached to the surface of large ones, explaining the observed free millimeter-sized particles with relatively low abundance. Our results suggest that studies of small particles in Saturn's rings would provide constraints on the cohesive force between icy particles, which is important not only for the origin and evolution of planetary rings but also for other astrophysical problems including dust evolution and planetesimal formation in protoplanetary disks.

Keywords: Planetary rings — Saturn, rings — Collisional physics

1. INTRODUCTION

Saturn's rings are more than 90 to 95 per cent water ice (Cuzzi et al. 2010), and size distribution of particles in the rings is expected to provide us clues to their origin and evolution. The first detailed information about the size distribution of particles in Saturn's rings was obtained by the radio occultation experiment by Voyager 1, where the radio source onboard the spacecraft was used to measure the radio opacity at two wavelengths, 3.6 cm and 13 cm (Marouf et al. 1983; Zebker et al. 1985). Also, measurements of the differential scattering cross section and integral inversion were used to derive the distribution of particle radius R for 1m $\leq R \leq$ 15 m. The results showed that the size distribution can be approximated by a power-law $n(R) = n_0(R/R_0)^{-q}$ with $q \simeq 3$ for centimeter- to meter-size particles, while there is an upper cutoff in the size distribution at $R \simeq 5$ m. The tendency of increasing q from the inner to outer A ring was also found.

On the other hand, Showalter and Nicholson (1990) estimated the size of the largest particles by an analysis of the statistical properties of the Voyager PPS stellar occultation data. In this case, the excess variance of the photon counts during stellar occultation is used to constrain the size of large particles. They found that the effective particle radius is about $2 - 10$ m in the main rings. Furthermore, French and Nicholson (2000) derived size distribution from ground-based observations of the 3 July 1989 occultation of 28 Sgr and the Voyager photopolarimeter subsystem (PPS) optical depth profile. They used the PPS occultation data (Esposito et al. 1983) to estimate and then remove the directly transmitted signal from the star, and derived parameters for the assumed power-law particle size distribution from the scattered light profiles at wavelengths of 0.9, 2.1, and 3.9 μm together with a forward-scattering model. They found that the maximum particle radius to be $R_{\rm max} \simeq 10$ m and 20m for the C ring and other ring regions, respectively, while $R_{\rm min} \simeq 30$ cm for the inner A ring and the B ring and $R_{\rm min} \simeq 1$ cm for the C ring and the outer A ring, respectively. French and Nicholson (2000) also calculated the effective particle radius defined by Showalter and Nicholson (1990) for the size distribution they obtained from their observation, and found agreement with Showalter and Nicholson (1990). More recently, Colwell et al. (2018) applied a method similar to Showalter and Nicholson (1990) to Cassini Ultraviolet Imaging Spectrograph (UVIS) occultation data, and examined radial variation of the effective particle size in detail.

Voyager observations as well as ground-based observations provided us information about particles down to sizes of the order of 1 cm, but information about the size distribution of sub-centimeter particles has been rather limited. While micron-sized particles are found in some locations of the main rings such as transient spokes or narrow diffuse rings (e.g., Mitchell et al. 2013; Hedman et al. 2010), observations show that their amount in the main rings is rather limited (Dones et al. 1993; Harbison et al. 2013). In Cassini's radio science occultation experiment (Marouf et al. 2008; Cuzzi et al. 2009), the use of three radio bands (1.3 cm, 3.6 cm, and 13 cm) allowed estimate of the minimum particle radius $R_{\rm min} \simeq 4$ mm and $\simeq 5$ mm for the C and A rings, respectively, although the cutoff

need not to be an actual sudden drop in the size distribution to explain the observation (Cuzzi et al. 2009).

Recently, some alternative approaches based on Cassini observations have been used to derive constraints on the size of the smallest particles in Saturn's rings. Harbison et al. (2013) used solar occultation data obtained by the Visual and Infrared Mapping Spectrometer (VIMS) onboard Cassini, and measured light forward scattered by particles in the A and C rings. Assuming a power-law size distribution with the slope index constrained by the radio occultation data, they estimated the size of the smallest particles in the C ring to be $R_{\rm min} \simeq 4$ mm, and for the A ring $R_{\rm min} \simeq 0.3 - 0.6$ mm depending on the assumed values of q. Becker et al. (2016) used data of diffraction spikes near the edges of the Encke Gap and the outer edge of the A ring observed by Cassini's UVIS High Speed Photometer (HSP) during stellar occultations to derive constraints on particle size distribution. Comparing the observed data with those obtained by a forward model that reconstructs the geometry for each occultation and produces a synthetic diffraction signal, they found a tendency of increasing q with increasing distance from Saturn, which is consistent with previous results. Also, they estimate $R_{\rm min}$ at the inner and outer edges of the Encke Gap and the outer edge of the A ring to be 15 mm, 9.3 mm, and 4.4 mm, respectively. Furthermore, Jerousek et al. (2016) combined UVIS and VIMS stellar occultation measurements with a geometric model of self-gravity wakes to extract information about the size of small particles in the rings. They found a significant fraction of sub-centimeter particles only in the outermost region of the A ring. A trend of increasing abundance of such small particles from the Encke Gap region to the outer edge of the A ring was also found.

These observational results provide us a view that the size distribution of particles in Saturn's rings can be approximated by a power-law from several meters down to sizes of the order of 1cm, with a significant amount of smaller particles down to ~ 1 mm. They also show that the contribution of sub-centimeter particles to the optical depth is relatively little (Harbison et al. 2013), which could be explained by a shallower power-law in that size regime. Dones et al. (1993) argued that the observed small contribution of sub-centimeter particles to the optical depth would be explained by cohesive

forces. Because smaller particles have larger surface-to-volume ratios, such forces are more effective for smaller ones. Theoretical models for collision of icy small particles including the cohesive force have been developed (e.g. Chokshi et al. 1993; Brilliantov et al. 1996; Spahn et al. 2004; Brilliantov et al. 2007) based on the so-called JKR theory (Johnson et al. 1971). These models were also applied to examine dynamical evolution of ring particles, such as the stability of aggregates in Saturn's rings (Albers and Spahn 2006) or the slope and upper cut-off of the particle size distribution (Brilliantov et al. 2015).

As for the smallest size of particles in Saturn's rings, using the cohesion model by Chokshi et al. (1993), Dones et al. (1993) analytically showed that sub-centimeter particles can stick to the surface of larger ones in unperturbed regions of the rings. More recently, Bodrova et al. (2012) developed a simple theoretical model for cohesion and release of small particles on the surface of larger ones in Saturn's rings, on the basis of the JKR theory for the cohesive forces. Assuming a bimodal size distribution for ring particles, they calculated rates of cohesion and release of small particles, and obtained steady-state abundance of free small particles. Their results explained the paucity of sub-centimeter particles in unperturbed regions of Saturn's rings. They also showed that increased velocity dispersion of particles would significantly enhance the fraction of free small particles. Bodrova et al. (2012) estimated impact velocity between ring particles using analytic consideration of particles' velocity dispersion, but the impact velocity can be significantly smaller than the velocity dispersion in dense rings, where particles tend to move coherently forming gravitational wakes (e.g. Salo 1995; Daisaka and Ida 1999). Although Bodrova et al. (2012) considered a wide range of impact velocities, a more detailed modeling is desirable to better understand the size distribution of particles in Saturn's rings inferred from recent Cassini observations.

In the present work, using N-body simulation, we examine impact velocities of macroscopic particles in unperturbed regions of Saturn's rings in detail. We examine cases for different radial locations in the main rings, and also investigate effects of varying parameters, such as optical depth, restitution coefficient, and particle size distribution. Then, on the basis of our simulation results, we discuss

expected minimum size of particles that can avoid sticking onto the surface of larger particles for an assumed strength of the cohesive force. First, in Section 2, we describe our numerical method, and present numerical results for impact velocities between particles. Using our numerical results, in Section 3, we discuss expected size of the smallest free particles in unperturbed regions of Saturn's main rings for an assumed strength of the cohesive force. Summary and discussion are given in Section 4.

2. IMPACT VELOCITY BETWEEN RING PARTICLES

2.1. *Numerical Method*

We carry out local N-body simulation with the code developed by Daisaka et al. (2001) and used in our previous works (Ohtsuki et al. 2013; Yasui et al. 2012, 2014). In this simulation, employing a periodic boundary conditions, gravitational forces from particles in adjacent cells are calculated (Salo 1995; Daisaka et al. 2001). In the case of dense self-gravitating rings, the size of the rectangular simulation cell (L) is chosen so that it satisfies $L \geq 4\lambda_{\rm cr}$ (Salo 1995), where

$$\lambda_{\rm cr} = 4\pi^2 G\Sigma/\Omega^2 \tag{1}$$

is the critical wavelength for gravitational instability for rings with surface density Σ and Keplerian orbital frequency Ω. When a collision between particles is detected, velocity changes of the colliding particles are calculated with the hard-sphere model (Richardson 1994; Ohtsuki and Emori 2000; Daisaka et al. 2001). We assume that particles have smooth spheres, and spins of particles are not taken into account. As for the normal restitution coefficient $\varepsilon_{\rm n}$, we examine the following four cases (Fig. 1): (i) $\varepsilon_{\rm n} = 0.1$; (ii) the velocity-dependent restitution coefficient based on Bridges et al. (1984) given as

$$\varepsilon_{\rm n}(v) = \min\left\{0.32(v_{\rm n}/v_{\rm c})^{-0.234}, 1\right\}, \tag{2}$$

where $v_{\rm n}$ is the normal component of impact velocity and $v_{\rm c} = 1{\rm cm\ s^{-1}}$ $(\equiv v_{\rm B})$; (iii) the expression (2) with $v_{\rm c} = 0.25 v_{\rm B}$; and (iv) the expression (2) with $v_{\rm c} = 5 v_{\rm B}$. In most of our self-gravitating simulations we assume that the material density of the particles is $\rho = 0.4$ g cm^{-3} (e.g. Porco et al. 2008), and the dependence on the material density will be examined in Section 2.4.

In the present work, we examine impact velocity between particles using this local simulation. After the system reaches a quasi-steady state, we record impact velocity $v_{\rm imp} = |\boldsymbol{v}_2 - \boldsymbol{v}_1|$ ($\boldsymbol{v}_1$ and $\boldsymbol{v}_2$ are the velocity of the colliding particles) for each collision, and examine their average, distribution, and maximum value. First, we examine cases of equal-sized particles, with and without self-gravity (Sections 2.2 and 2.3). The case with size distribution is discussed in Section 2.4.

2.2. *Velocity Dispersion and Impact Velocity*

Particles in Saturn's rings have velocity dispersion due to collision and gravitational interactions between them. The radial and vertical components of the velocity dispersion are related to the r.m.s. eccentricity and inclination as

$$\sigma_r = \sqrt{\frac{\langle e^2 \rangle}{2}} a\Omega, \qquad \sigma_z = \sqrt{\frac{\langle i^2 \rangle}{2}} a\Omega, \tag{3}$$

where a is the semi-major axis. N-body simulation shows that $\sigma_r \sim 2\sigma_z$ for dilute rings with $\tau \ll 1$, where τ is the optical depth (Ohtsuki and Emori 2000).

Bodrova et al. (2012) estimated impact velocity between ring particles from analytic estimates of their velocity dispersion. In the case of rings with equal-sized particles, the velocity dispersion can be analytically estimated based on results of N-body simulation, as follows (Salo 1995; Ohtsuki 1999; Ohtsuki and Emori 2000; Bodrova et al. 2012). When the optical depth is sufficiently low and mutual gravity between particles can be neglected, the velocity dispersion is determined by mutual collisions, and is approximately given as

$$\sigma_{\rm col} \sim 2R\Omega \sim 0.039 \left(\frac{R}{100{\rm cm}}\right) \left(\frac{a}{10^{10}\ {\rm cm}}\right)^{-3/2}\ {\rm cm\ s^{-1}}. \tag{4}$$

When $\tau \ll 1$ but particles' mutual gravity becomes important, the velocity dispersion is enhanced by their gravitational encounters, and is on the order of their mutual escape velocity, as

$$\sigma_{\rm enc} \sim v_{\rm esc} = \sqrt{\frac{2Gm}{R}}, \tag{5}$$

where m is the mass of the particle. Assuming that particles are spheres with density ρ, we have

$$\sigma_{\rm enc} \sim \sqrt{\frac{8\pi G\rho}{3}} R = 0.047 \left(\frac{\rho}{0.4{\rm g\ cm^{-3}}}\right)^{1/2} \left(\frac{R}{100{\rm cm}}\right)\ {\rm cm\ s^{-1}}. \tag{6}$$

On the other hand, gravitational wakes are formed in sufficiently dense rings. In this case, N-body simulation shows that the velocity dispersion is determined so that $Q_{\rm T} \sim 2$, where $Q_{\rm T} \equiv \sigma_r \Omega/(3.36G\Sigma)$ is the Toomre parameter (Salo 1995). From this relation, the velocity dispersion in this case can be estimated as

$$\sigma_{\rm wake} \sim 0.23 \left(\frac{\Sigma}{100{\rm g\ cm^{-2}}}\right) \left(\frac{a}{10^{10}{\rm cm}}\right)^{3/2}\ {\rm cm\ s^{-1}}. \tag{7}$$

Figure 2 shows the radial component of velocity dispersion and the mean impact velocity obtained by N-body simulation as a function of the dynamical optical depth τ for rings of equal-sized particles ($R = 100$ cm) located at $a = 1 \times 10^{10}$ cm from Saturn. Panels a and b show the case of rings with non-gravitating particles, while particles' self-gravity is taken into account in panels c and d. In each panel of Figure 2, results for four kinds of restitution coefficients (Fig. 1) are shown. In the non-gravitating case, the velocity dispersions decrease with increasing optical depth due to suppressed mobility of densely-packed particles (Wisdom and Tremaine 1988). The behavior of the mean impact velocity is similar to the velocity dispersion in the non-gravitating case, with $\langle v_{\rm imp} \rangle \simeq 2\sigma_r$. In the self-

gravitating case, $\sigma_r \sim \sigma_{\rm enc}$ for dilute rings and $\sigma_r \sim \sigma_{\rm wake}$ for dense rings with sufficiently dissipative particles, as reported in previous works (Salo 1995; Ohtsuki and Emori 2000). On the other hand, we find that the behavior of the mean impact velocity is very similar to the non-gravitating case. This is because in the self-gravitating case, particles in gravitational wakes tend to move coherently with relative velocities similar to the non-gravitating case (see also Salo 1995; Daisaka and Ida 1999). In the self-gravitating case, the importance of mutual gravity between particles relative to collision is described by the ratio of the mutual Hill radius ($R_{\rm H}$) for a pair of particles to the sum of their physical radii:

$$r_h = \frac{R_{\rm H}}{R_1 + R_2} = \left(\frac{4\pi\rho}{9M_{\rm S}}\right)^{1/3} a\frac{(1+\mu)^{1/3}}{1+\mu^{1/3}}, \tag{8}$$

where $M_{\rm S}$ is the mass of Saturn; R_1 and R_2 are the radii of the particles; and $\mu = m_1/m_2$ is their mass ratio. In the present case ($a = 1 \times 10^{10}$ and $\rho = 0.4$ g cm^{-3}), $r_h = 0.63$.

In the non-gravitating case, both velocity dispersion and mean impact velocity take on larger values when particles are more elastic. In the self-gravitating case, the dependence of the velocity dispersion on restitution coefficient is similar to the non-gravitating case when $\tau < 1$, while for $\tau > 1$ the velocity dispersion tends to be smaller for more elastic particles, because the tendency of the formation of gravitational wakes is suppressed by increased random velocity. On the other hand, the dependence of the impact velocity on the restitution coefficient is similar to the non-gravitating case.

Impact velocities have some distribution, which will be examined in detail in the next subsection. Here we focus on their maximum values, because high-velocity impacts would release small particles strongly attached to the surface of large ones, and the maximum impact velocity is related to the size of the smallest free particles in the rings (Section 3). Figure 3 shows the plots of the maximum impact velocity $v_{\rm imp,max}$ obtained in each simulation after the system reached a quasi-steady state as a function of optical depth, for the self-gravitating case shown in Figures 2c and 2d. Except for the case of the most elastic particles (i.e., the case of Eq.(2) with $v_{\rm c} = 5v_{\rm B}$), the behavior is rather insensitive to restitution coefficient. In the case of low optical depth, impacts at the highest velocity occur for particles in the high-velocity tail of the velocity distribution. We find that $v_{\rm imp,max}$

in this case is several times the mutual escape velocity of the particles. On the other hand, the maximum impact velocity in dense rings arises when adjacent wakes collide with each other (see also Figure 5 in §2.3). In this case, the maximum impact velocity can be roughly estimated by the Kepler shear between two adjacent wakes, i.e., $\sim \lambda_{\rm cr}\Omega$, where $\lambda_{\rm cr}$ is given by Eq.(1). We find that the numerical results for sufficiently dissipative particles shown in Fig. 3 can be well approximated by $v_{\rm imp,max} \sim \max\{6v_{\rm esc}, 0.4\lambda_{\rm cr}\Omega\}$, which is shown with the dotted line in the figure. Since $\lambda_{\rm cr}\Omega \propto \Sigma a^{3/2}$, it is expected that the maximum impact velocity between particles due to impacts between adjacent wakes is larger for denser ring and at outer parts of the rings.

2.3. *Distribution of Impact Velocities*

Next, we examine distribution of impact velocities (Fig. 4). We assume that all the particles have the same radius, $R = 100$ cm. Cases with particle size distribution will be discussed in Section 2.4. We examine the following three cases by varying the distance from the planet a and the optical depth τ: (i) $a = 1.28 \times 10^{10}$ cm and $\tau \simeq 0.77$, (ii) $a = 1.05 \times 10^{10}$ cm and $\tau \simeq 2$, and (iii) $a = 0.85 \times 10^{10}$ cm and $\tau \simeq 0.1$. These three cases roughly correspond to the A, B, and C rings, and the values of the r_h parameter defined by Equation (8) are (a) 0.80, (b) 0.66, and (c) 0.53, respectively. We showed in Section 2.1 that the velocity dispersion as well as the maximum impact velocity in dense rings increase with increasing optical depth, or surface density of the ring. From the analysis of weak linear density waves in the mid-A ring observed in Cassini images, Tiscareno et al. (2007) estimated the surface density in this region to be $\Sigma \simeq 43$ g cm^{-2}. On the other hand, using a wavelet-based analyses of Cassini's VIMS stellar occultation observations, Hedman and Nicholson (2016) estimated the surface density of the B ring to be between 40 and 140 g cm^{-2}. The above optical depths in our simulation were chosen to be consistent with these observations ($\Sigma \simeq 43$ g cm^{-2} for the A ring and $\Sigma \simeq 109$ g cm^{-2} for the B ring). As for the case of the B ring, we briefly discuss the dependence on the surface density in the next subsection.

In each panel of Figure 4, results for the four kinds of restitution coefficient are shown. These plots are created from the data recorded for each collision during the last one orbital period of each simulation. We find that the distributions of impact velocities for the cases of the A and B rings are similar. Most impacts take place at low velocities with $v_{\rm imp} \lesssim 0.1 - 0.2$ cm s^{-1}, because particles in gravitational wakes move coherently (Salo 1995; Daisaka and Ida 1999). On the other hand, high-velocity impacts with $v_{\rm imp} \gtrsim 0.3$ cm s^{-1} can also occur occasionally when adjacent wakes collide with each other, as shown in Figure 5. We also find a weak dependence on the restitution coefficient. In the case of the most elastic particles (i.e., the case with Eq.(2) with $v_{\rm c} = 5v_{\rm B}$) in the A and B rings, the maximum impact velocity is significantly smaller than the other ones. This is because formation of gravitational wakes is suppressed in such a relatively elastic case. On the other hand, the distribution of impact velocities in the dilute C ring is very different, as shown in Fig. 4c. In this case, unless particles are very (probably unrealistically) elastic, impact velocities distribute in a rather narrow range. Most impacts take place at low velocity with $v_{\rm imp} < 0.1$ cm s^{-1}, i.e., at velocities on the order of $\sigma_{\rm col}$ given by Eq. (4). The highest impact velocity is $0.3 - 0.5$ cm s^{-1} (i.e., several times the escape velocity), depending on the restitution coefficient.

2.4. *Case with Particle Size Distribution*

Next, we examine cases with particle size distribution. We assume a power-law size distribution with $n(R)dR \propto R^{-3}dR$ for 30 cm $\leq R \leq$ 300 cm. Although the size distribution of particles in Saturn's rings is likely much wider than this (Section 1), we can see some important characteristics for the case of size distribution even with the above assumption. Figure 6 shows the velocity dispersions and the mean impact velocities as a function of particle size for the three cases corresponding to the A, B, and C rings. These plots are created by grouping particles into ten logarithmic size bins and taking averages within each bin.

First, in the case of the dilute C ring, the velocity dispersion increases with decreasing particle size, owing to the tendency of equipartition of kinetic energy among particles with different sizes (Ohtsuki

1999, 2006; Morishima and Salo 2006). Similar tendency can be seen in the case of relatively elastic particles for the A and B rings, where the velocity dispersions slightly increase with decreasing particle size, because small particles are easily stirred by gravitational wakes and/or large particles. This tendency is reduced in dense rings when collisions are more dissipative, because highly dissipative collisions lead even small particles to move coherently with other particles in wakes (Fig. 7; see also Porco et al. (2008)).

In the case of the dilute C ring, the mean impact velocity can be approximated by $\sigma_{\rm col}$, while the maximum value is roughly several times the escape velocity of the largest particles. These values are similar to the case of equal-sized particles shown in Fig. 4. On the other hand, we find that the dependence of mean impact velocities on particle size and restitution coefficient is rather weak in the case of the A and B rings, except for the case of the most elastic particles. Again, this is because most particles move coherently in gravitational wakes with low relative velocity. We examined maximum values of impact velocity in these cases with size distribution and found that they show rather weak size-dependence. Larger particles tend to have small velocity dispersions, but they also experience rather high-velocity impacts with small ones. Typical values of the mean impact velocity in these dense rings are $v_{\rm imp} < 0.1$ cm s^{-1}, and we found $v_{\rm imp,max} \simeq 1-2$ cm s^{-1}, although high-velocity impacts with $v_{\rm imp} \gtrsim 0.5$ cm s^{-1} are rather rare (see also Figures 4a, 4b, and 5).

Since the surface density of the dense B ring obtained by observations has some uncertainty (Hedman and Nicholson 2016; Robbins et al. 2010), we also examined the dependence of the mean impact velocity on the surface density, and found that it is similar to the case of equal-sized particles (Figure 2d); the mean impact velocity decreases with increasing surface density owing to the suppressed mobility of particles, while it is rather insensitive to the surface density when the ring is sufficiently dense to form gravitational wakes. We also examined the dependence on the material density of particles, ρ, in the case of dense self-gravitating rings. When ρ is higher, enhanced effects of mutual gravity between particles lead to the increase in velocity dispersions, especially for small particles (Figure 8). Similar behavior was found when the distance from the planet is increased with a fixed

particle density (Morishima and Salo 2006). On the other hand, we found that impact velocities are hardly changed for the range of particle densities examined ($\rho = 0.4 - 0.9$ g cm^{-3}), because in all these three cases gravitational wakes are more or less formed and particles tend to move coherently.

3. IMPLICATIONS FOR MINIMUM PARTICLE SIZE

As we mentioned in Section 1, the cohesive force between particles has been proposed as a mechanism to explain the paucity of sub-centimeter particles in Saturn's rings (Dones et al. 1993; Bodrova et al. 2012). On the basis of the JKR theory for the cohesive force (Johnson et al. 1971; Chokshi et al. 1993), Bodrova et al. (2012) developed a simple model for sticking and release of small particles on the surface of large particles in Saturn's rings. While the effects of the cohesive force becomes more important for small particles, impact velocity has to be sufficiently low in order for them to stick by the cohesive force to the surface of large ones. This gives a minimum size of small particles that can avoid sticking for a given impact velocity as (Appendix A)

$$R_{\rm stc} = C_1 \left(\frac{\gamma^5 (1-\nu^2)^2}{v_{\rm imp}^6 \rho^3 E^2} \right)^{1/5}, \tag{9}$$

where $C_1 \simeq 2.97$; γ is the adhesion energy per unit area (Israelachvili 2011; Bodrova et al. 2012); and ρ, ν, and E are the density, Poisson's ratio, and Young's modulus of particles, respectively.

On the other hand, from the condition that the attached small particles leave the surface of large ones at collision between large ones, another criterion for the minimum size of free small particles can be derived. Employing a simple model, Bodrova et al. (2012) calculated the maximum inertial force acting at collision between large particles on attached small particles, and derived the minimum impact velocity between large particles that lead to the release of small particles from their surface. On the basis of their model, we can derive the minimum size of particles that can detach from the surface of large particles with radius $R_{\rm L}$ when the large particles collide with each other at velocity $v_{\rm imp}$ as (Appendix A)

$$R_{\rm det} = C_2 \left(\frac{\gamma^5 (1-\nu^2)^2 R_{\rm L}^5}{v_{\rm imp}^6 \rho^3 E^2} \right)^{1/10}, \tag{10}$$

where $C_2 \simeq 1.89$. In the above, we have assumed that the small particles is much smaller than the large ones.

As for the adhesion energy per unit area for pure ice surfaces, Chokshi et al. (1993) estimated $\gamma = 0.74$ J m^{-2}, while more recently laboratory experiments were carried out to evaluate this quantity. Here we use $\gamma = 0.38$ J m^{-2}, which is twice the surface energy experimentally obtained for micron-sized ice particles (Gundlach et al. 2011; Bodrova et al. 2012), although the strength of the cohesive force for actual ring particles is largely unknown. Also, following Bodrova et al. (2012), we assume $\nu = 0.25$, $E = 7 \times 10^9$ Pa, and $\rho = 0.9$ g cm^{-3} in Equations (9) and (10).

In Figure 9, we plot $R_{\rm stc}$ as a function of $v_{\rm imp}$. If particles are smaller than $R_{\rm stc}$, such small particles hitting a large one with impact velocity $v_{\rm imp}$ can stick to the surface of the latter, while they rebound without sticking if the size is larger than this critical value. We also show the plots of $R_{\rm det}$ for the three cases of the size of the large particles ($R_{\rm L} = 1$cm, 10cm, and 100cm). If the size of the small particles is smaller than $R_{\rm det}$, they remain on the surface of the large ones at collision between the large ones, while at least some of small particles are detached from the surface owing to insufficient cohesive force if their size is larger than this critical value.

In this figure, we also show the range of impact velocities of ring particles in Saturn's A, B, and C rings estimated from the results of our present study. As we mentioned in Section 2, most collisions take place at low velocities ($\lesssim 0.1$ cm s^{-1}), while infrequent high-velocity impacts also occur. In the dense A and B rings, impacts with $v_{\rm imp} \simeq 0.3 - 0.5$ cm s^{-1} occasionally occur, with the maximum impact velocity being $\sim 1 - 2$ cm s^{-1} (Figures 4a, 4b, and 5). In the case of the C ring, on the other hand, the maximum impact velocity is ~ 0.5 cm s^{-1} when collisions are sufficiently dissipative (Fig. 4c).

From these results, we can infer the size of the smallest free particles, i.e., those detached from the surface of large ones. In all the three main rings, impacts between particles at low velocity with $v_{\rm imp} \lesssim 0.1$ cm s^{-1} frequently take place. For example, when $v_{\rm imp} = 0.05$ cm s^{-1}, we have $R_{\rm stc} \simeq 1$cm, i.e., particles smaller than 1 cm are expected to stick to the surface of large particles. On the other hand, Figure 9 shows that $R_{\rm det} \simeq 1$cm for $R_{\rm L} = 1$cm, i.e., such low-velocity impacts are sufficient to release particles with $R \gtrsim 1$ cm from large ones, while smaller particles remain attached to the surface of large ones. This is consistent with the observed paucity of sub-centimeter particles in the main rings, as discussed in previous works (Dones et al. 1993; Bodrova et al. 2012).

On the other hand, although less frequent, collisions with sufficiently high velocities to detach smaller particles also take place. For such high-velocities, we find that $R_{\rm stc} \simeq 1$mm, i.e., only millimeter-sized or smaller particles can stick to the large ones. Figure 9 shows that $R_{\rm det} \simeq 1-5$mm for $R_{\rm L} = 1$cm in such a case. This means that among sub-centimeter particles that stick to the large ones at low-velocity impacts, those with $R \simeq 1-5$mm will be released at high-velocity impacts between large particles with $R_{\rm L} \simeq 1$cm. Most of those released sub-centimeter particles are expected to stick on the surface of large particles at subsequent low-velocity impacts, but some would avoid sticking due to infrequent high-velocity impacts. As a result, free millimeter-sized particles are expected to be present in these rings. Because such high-velocity impacts are not as frequent as low-velocity impacts, the abundance of free sub-centimeter particles is expected to be significantly lower than larger ones. These seem to be consistent with the results of recent studies on the smallest size of ring particles based on Cassini observations (Harbison et al. 2013; Becker et al. 2016; Jerousek et al. 2016).

4. CONCLUSIONS AND DISCUSSION

Recent studies based on Cassini observations have provided detailed information about size distribution of particles in Saturn's rings. These studies suggest that it can be approximated by a power-law from several meters down to sizes of the order of 1cm, with a significant amount of smaller

particles down to ~ 1 mm. They also show that the contribution of sub-centimeter particles to the optical depth is relatively little due to the shallower power-law in that size regime (Section 1).

In order to better understand these observations, we examined impact velocities between particles using N-body simulation. Below is the summary of our simulation and analytic consideration on particle impact velocity.

- Mean impact velocity between particles in Saturn's main rings is rather low ($v_{\rm imp} \lesssim 0.1$ cm s^{-1}). This is true even in dense rings such as the A and B rings where particles' velocity dispersions are enhanced by gravitational wakes, because particles tend to move coherently in wakes. As a result, the mean impact velocity between particles in dense rings is significantly smaller than their analytically-estimated velocity dispersion (Eq.(6)).

- Maximum impact velocity $v_{\rm imp,max}$ in dilute rings is several times the mutual escape velocity, while it is on the order of the Kepler shear velocity between adjacent wakes in dense rings. The latter high-velocity impacts in dense rings arise when two adjacent wakes collide with each other, and the impact velocity in such cases is expected to be larger for denser rings and at outer parts of the rings.

- In the case of particles with size distribution, we found that the dependence of impact velocities on particle size is rather weak, unless particles are very elastic. This is mainly because particles experience collisions with various sizes of particles. In the case of dense rings, the fact that most particles move coherently in wakes also reduces the size-dependence of impact velocity.

- The above results imply that most impacts in Saturn's main rings take place at low velocities ($\lesssim 0.1$ cm s^{-1}). Also, impact velocities distribute over a wide range, and the velocities of infrequent high-velocity impacts are significantly larger than the analytically-estimated velocities dispersions (Eqs.(4), (5), and (6)). In the case of the A and B rings, impacts with $v_{\rm imp} \simeq 0.3 - 0.5$ cm s^{-1} occasionally occur, with $v_{\rm imp,max} \simeq 1 - 2$ cm s^{-1}, while in the C ring $v_{\rm imp,max} \lesssim 0.5$ cm s^{-1} as long as collisions are sufficiently dissipative (Figure 9).

On the basis of the results of these simulations, we examined minimum size of free ring particles that can avoid sticking onto the surface of larger ones. We found that the typical impact velocity of particles in the main rings is too low to detach sub-centimeter particles that are attached to the surface of large ones due to the cohesive force, explaining their paucity in the main rings (Dones et al. 1993; Bodrova et al. 2012). On the other hand, infrequent high-velocity impacts can release millimeter-sized particles strongly attached to the surface of large ones, explaining the observed free millimeter-sized particles with relatively low abundance. These results seem to be consistent with recent studies on the estimate of the size of the smallest particles in Saturn's rings base on Cassini observations (e.g., Harbison et al. 2013; Becker et al. 2016, see Section 1). In the present work, we examined impact velocities between particles in unperturbed rings. Satellite perturbations are expected to increase velocity dispersion as well as impact velocity, and the abundance of smaller particles is expected to increase such perturbed regions (Bodrova et al. 2012; Jerousek et al. 2016).

In the present work, we derived the critical particle sizes for sticking and collisional release based on the simple model described in Bodrova et al. (2012). These critical sizes depend on the assumed strength of the cohesive force (Eqs.(9) and (10)). We used the value of the cohesive force based on the laboratory experiments for micron-sized particles (Gundlach et al. 2011). Our estimates of the size of the smallest ring particles based on the above assumptions seem roughly consistent with Cassini observations, as mentioned above, although the actual cohesive strength in the ring environment is poorly constrained. Cohesive strength between small icy particles is an important quantity not only in the origin and evolution of planetary rings but also in other astrophysical problems including dust evolution and formation of planetesimals in protoplanetary disks (Testi et al. 2014). Our present work suggests that constraints on this important quantity could be obtained by further observational and/or theoretical studies of Saturn's rings.

This work was supported by JSPS KAKENHI Nos. 15H03716, 16H04041, and 18K11334. Part of the numerical simulations were performed using computer systems at the National Astronomical Observatory of Japan.

APPENDIX

A. ANALYTIC ESTIMATE OF THE CRITICAL SIZE OF RING PARTICLES FOR STICKING AND COLLISIONAL RELEASE

Here, we analytically derive minimum size of ring particles that can avoid sticking onto the surface of large particles, on the basis of previous works (Johnson et al. 1971; Chokshi et al. 1993; Spahn et al. 2004; Bodrova et al. 2012).

First, we derive the condition for the sticking of small particles on the surface of large ones. Let the mass and radius of the small particles be $m_{\rm S}$ and $R_{\rm S}$, and those of the large ones be $m_{\rm L}$ and $R_{\rm L}$. The force acting between the small and large particles during the collision can be given based on the so-called JKR theory (Johnson et al. 1971) as

$$F = \frac{a^3}{DR} - \sqrt{\frac{6\pi\gamma}{D}} a^{3/2}, \tag{A1}$$

where a is the contact radius of the colliding particles; $D = (3/2)(1-\nu^2)/E$ with ν and E being Poisson's ratio and Young's modulus, respectively; $R = R_{\rm S}R_{\rm L}/(R_{\rm S}+R_{\rm L})$ is the reduced radius of the two particles; and γ is the adhesion energy per unit area (Israelachvili 2011; Bodrova et al. 2012), which is twice the surface energy.

Let the total displacement due to their deformation of the surfaces of the two particles during collision be ξ ($= R_{\rm S} + R_{\rm L} - |\boldsymbol{r}_{12}|$, where $\boldsymbol{r}_{12}$ is the vector connecting the centers of the colliding particles). Then, ξ can be expressed as a function of a as (Bodrova et al. 2012)

$$\xi = \frac{a^2}{R} - \sqrt{\frac{8}{3}\pi\gamma D a}. \tag{A2}$$

The contact radius and the displacement in the equilibrium ($F = 0$) can be written as

$$\begin{aligned} a_0 &= (6\pi\gamma D R^2)^{1/3} \\ \xi_0 &= \frac{1}{3}(6\pi\gamma D R^{1/2})^{2/3}. \end{aligned} \tag{A3}$$

When the two particles collide, ξ increases until it takes on its maximum value, where the direction of their relative velocity changes. Then, after passing the equilibrium point ($\xi = \xi_0$), the force F takes on its minimum value, and the two particles become separated soon after that if the cohesive force is not sufficiently strong to keep them attached with each other. If we assume that their separation takes place when F takes on its minimum value (Bodrova et al. 2012), the contact radius immediately before separation can be derived from $dF/da = 0$ as

$$a_{\text{sep}} = \left(\frac{3}{2}\pi\gamma D R^2\right)^{1/3}, \tag{A4}$$

and the force acting between the two particles at this moment is

$$F_{\text{sep}} = \frac{3}{2}\pi\gamma R. \tag{A5}$$

The work required to release a bound particle from its equilibrium position can then be calculated as (Bodrova et al. 2012)

$$\begin{aligned} W_{\text{el}} &= \int_{a_0}^{a_{\text{sep}}} F \frac{d\xi}{da} da \\ &= q_0 \left(\pi^5 \gamma^5 D^2\right)^{1/3} R^{4/3}, \end{aligned} \tag{A6}$$

where $q_0 \simeq 1.457$. Therefore, if the relative kinetic energy between the two particles at the end stage of collision is larger than $W_{\rm el}$, the two particles can become separated. This leads to the size of the smallest particles that can avoid sticking onto the surface of the large ones for a given impact velocity $v_{\rm imp}$. If we assume $R_{\rm s} \ll R_{\rm L}$, we can derive the critical size of the small particles for sticking from the condition $W_{\rm el} = m_{\rm S} v_{\rm imp}^2/2$ as

$$R_{\rm stc} = C_1 \left(\frac{\gamma^5 (1-\nu^2)^2}{v_{\rm imp}^6 \rho^3 E^2} \right)^{1/5}, \tag{A7}$$

where $C_1 = 3\pi^{2/5} q_0^{3/5}/2 \simeq 2.97$. That is, when a small particle collide with a large one at impact velocity $v_{\rm imp}$, they stick together when $R_{\rm S} < R_{\rm stc}$, while they rebound when $R_{\rm S} > R_{\rm stc}$.

On the other hand, those small particles attached onto the large ones can detach from their surface at collision between large ones. Bodrova et al. (2012) estimated the inertial force acting on the attached small particles at collision between the large ones, and considered that the small ones detach from the large ones if the inertial force overcomes the cohesive force.

According to their model, the inertial force on the small one becomes the largest when the contact displacement ξ takes on its maximum value ($\xi_{\rm max}$). The elastic force acting between the two colliding large particles can be expressed in terms of ξ as (Bodrova et al. 2012)

$$F_{\rm el} = \frac{\sqrt{R}}{D} \xi^{3/2}. \tag{A8}$$

Thus, the stored elastic energy at $\xi = \xi_{\rm max}$ is

$$W_{\rm el} = \int_0^{\xi_{\rm max}} F_{\rm el} d\xi = \frac{2\sqrt{R}}{5D} \xi_{\rm max}^{5/2}. \tag{A9}$$

If we neglect energy dissipation for simplicity, $\xi_{\rm max}$ can be obtained from $W_{\rm el} = m v_{\rm imp}^2/2$ as

$$\xi_{\max} = \left(\frac{5Dm}{4\sqrt{R}}\right)^{2/5} v_{\rm imp}^{4/5}. \tag{A10}$$

In the above, m is the reduced mass for the two colliding large particles. If we assume that they have the same mass $m_{\rm L}$, we have $m = m_{\rm L}/2$. The maximum inertial force acting on small particles attached on the surface of one of the colliding large particles is (Bodrova et al. 2012)

$$F_{\rm in,max} = \frac{F_{\rm el}(\xi_{\max})}{2m} m_{\rm S}. \tag{A11}$$

If the component of this inertial force in the direction perpendicular to the surface of the large particle one exceeds $F_{\rm sep}$ given by Eq.(A5), the attached small particles can be released (Bodrova et al. 2012). Thus, the minimum size of small particles ($R_{\rm det}$) that can detach from the surface of the large ones can be derived from $F_{\rm in,max} = F_{\rm sep}$. Assuming $R_{\rm S} \ll R_{\rm L}$, we obtain

$$R_{\rm det} = C_2 \left(\frac{\gamma^5 (1-\nu^2)^2 R_{\rm L}^5}{v_{\rm imp}^6 \rho^3 E^2}\right)^{1/10}, \tag{A12}$$

where $C_2 \simeq 1.89$. That is, those small particles attached to the surface of the large particles can be released at collision between large particles if $R_{\rm S} > R_{\rm det}$.

REFERENCES

Albers, N., Spahn, F. 2006. The influence of particle adhesion on the stability of agglomerates in Saturn's rings. Icarus 181, 292-301.

Becker, T. M., Colwell, J. E., Esposito, L. W., Bratcher, A. D. 2016. Characterizing the particle size distribution of Saturn's A ring with Cassini UVIS occultation data. Icarus 279, 20-35.

Bodrova, A., Schmidt, J., Spahn, F., Brilliantov, N. 2012. Adhesion and collisional release of particles in dense planetary rings. Icarus 218, 60-68.

Bridges, F. G., Hatzes, A., Lin, D. N. C. 1984. Structure, stability and evolution of Saturn's rings. Nature 309, 333-335.

Brilliantov, N. V., Spahn, F., Hertzsch, J.-M., Pöschel, T. 1996. Model for collisions in granular gases. Phys. Rev. E 53, 5382-5392.

Brilliantov, N. V., Albers, N., Spahn, F., Pöschel, T. 2007. Collision dynamics of granular particles with adhesion. Phys. Rev. E 76, 051302.

Brilliantov, N. V., Krapivsky, P. L., Bodrova, A., Spahn, F., Hayakawa, H., Stadnichuk, V., Schmidt, J. 2015. Size distribution of particles in Saturn's rings from aggregation and fragmentation. PNAS 112, 9536-9541.

Chokshi, A., Tielens, A. G. G. M., Hollenbach, D. 1993. Dust coagulation. Astrophys. J. 407, 806-819.

Colwell, J. E., Esposito, L. W., Cooney, J. H. 2018. Particle sizes in Saturn's rings from UVIS stellar occultations 1. Variations with ring region. Icarus 300, 150-166.

Cuzzi, J., Clark, R., Filacchione, G., French, R., Johnson, R., Marouf, E., Spilker, L. 2009. Ring particle composition and size distribution. Saturn from Cassini-Huygens 459.

Cuzzi, J. N., and 22 colleagues 2010. An evolving view of Saturn's dynamic rings. Science 327, 1470.

Daisaka, H., Ida, S. 1999. Spatial structure and coherent motion in dense planetary rings induced by self-gravitational instability. Earth, Planets, and Space 51, 1195-1213.

Daisaka, H., Tanaka, H., Ida, S. 2001. Viscosity in a dense planetary ring with self-gravitating particles. Icarus 154, 296-312.

Dones, L., Cuzzi, J. N., Showalter, M. R. 1993. Voyager Photometry of Saturn's A ring. Icarus 105, 184-215.

Esposito, L. W., Ocallaghan, M., West, R. A. 1983. The structure of Saturn's rings - Implications from the Voyager stellar occultation. Icarus 56, 439-452.

French, R. G., Nicholson, P. D. 2000. Saturn's rings II. Particle sizes inferred from stellar occultation Data. Icarus 145, 502-523.

Gundlach, B., Kilias, S., Beitz, E., Blum, J. 2011. Micrometer-sized ice particles for planetary-science experiments - I. Preparation, critical rolling friction force, and specific surface energy. Icarus 214, 717-723.

Harbison, R. A., Nicholson, P. D., Hedman, M. M. 2013. The smallest particles in Saturn's A and C Rings. Icarus 226, 1225-1240.

Hedman, M. M., Nicholson, P. D. 2016. The B-ring's surface mass density from hidden density waves: Less than meets the eye? Icarus 279, 109-124.

Hedman, M. M., Burt, J. A., Burns, J. A., Tiscareno, M. S. 2010. The shape and dynamics of a heliotropic dusty ringlet in the Cassini Division. Icarus 210, 284-297.

Israelachvili, J. N. 2011. *Intermolecular and Surface Forces, 3rd Edition*, Academic Press.

Jerousek, R. G., Colwell, J. E., Esposito, L. W., Nicholson, P. D., Hedman, M. M. 2016. Small particles and self-gravity wakes in Saturn's rings from UVIS and VIMS stellar occultations. Icarus 279, 36-50.

Johnson, K. L., Kendall, K., Roberts, A. D. 1971. Surface energy and the contact of elastic solids. Proceedings of the Royal Society of London Series A 324, 301-313.

Marouf, E. A., Tyler, G. L., Zebker, H. A., Simpson, R. A., Eshleman, V. R. 1983. Particle size distributions in Saturn's rings from Voyager 1 radio occultation. Icarus 54, 189-211.

Marouf, E. A., French, R., Rappaport, N., Wong, K., McGhee, C., Anabtawi, A. 2008. Physical properties of Saturn's rings from Cassini radio occultations. Bulletin of the American Astronomical Society 40, 24.02.

Mitchell, C. J., Porco, C. C., Dones, H. L., Spitale, J. N. 2013. The behavior of spokes in Saturn's B ring. Icarus 225, 446-474.

Morishima, R., Salo, H. 2006. Simulations of dense planetary rings. IV. Spinning self-gravitating particles with size distribution. Icarus 181, 272-291.

Ohtsuki, K. 1999. Evolution of particle velocity dispersion in a circumplanetary disk due to inelastic collisions and gravitational interactions. Icarus 137, 152-177.

Ohtsuki, K. 2006. Rotation rate and velocity dispersion of planetary ring particles with size distribution II. Numerical simulation for gravitating particles. Icarus 183, 384-395.

Ohtsuki, K., Emori, H. 2000. Local N-body simulations for the distribution and evolution of particle velocities in planetary rings Astron. J. 119, 403-416.

Ohtsuki, K., Yasui, Y., Daisaka, H. 2013. Accretion rates of moonlets embedded in circumplanetary particle disks. Astron. J. 146, 25.

Porco, C. C., Weiss, J. W., Richardson, D. C., Dones, L., Quinn, T., Throop, H. 2008. Simulations of the dynamical and light-scattering behavior of Saturn's rings and the derivation of ring particle and disk properties. Astron. J. 136, 2172-2200.

Richardson, D. C. 1994. Tree code simulations of planetary rings. Mon. Not. R. Astron. Soc. 269, 493-511.

Robbins, S. J., Stewart, G. R., Lewis, M. C., Colwell, J. E., Sremčević, M. 2010. Estimating the masses of Saturn's A and B rings from high-optical depth N-body simulations and stellar occultations. Icarus 206, 431-445.

Salo, H. 1995. Simulations of dense planetary rings. III. Self-gravitating identical particles. Icarus 117, 287-312.

Schmidt, J., Ohtsuki, K., Rappaport, N., Salo, H., Spahn, F. 2009. Dynamics of Saturn's dense rings. In *Saturn from Cassini-Huygens* (M. Dougherty et al. Eds.), Springer, pp. 413-458.

Showalter, M. R., Nicholson, P. D. 1990. Saturn's rings through a microscope - Particle size constraints from the Voyager PPS scan. Icarus 87, 285-306.

Spahn, F., Albers, N., Sremcevic, M., Thornton, C. 2004. Kinetic description of coagulation and fragmentation in dilute granular particle ensembles. Europhys. Lett. 67, 545-551.

Testi, L., and 10 colleagues 2014. Dust evolution in protoplanetary disks. In *Protostars and Planets VI* (H. Beuther et al. Eds.), Univ. Arizona Press, pp. 339-361.

Tiscareno, M. S., Burns, J. A., Nicholson, P. D., Hedman, M. M., Porco, C. C. 2007. Cassini imaging of Saturn's rings. II. A wavelet technique for analysis of density waves and other radial structure in the rings. Icarus 189, 14-34.

Wisdom, J., Tremaine, S. 1988. Local simulations of planetary rings. Astron. J. 95, 925-940.

Yasui, Y., Ohtsuki, K., Daisaka, H. 2012. Viscosity in planetary rings with spinning self-gravitating particles. Astron. J. 143, 110.

Yasui, Y., Ohtsuki, K., Daisaka, H. 2014. Gravitational accretion of particles onto moonlets embedded in Saturn's rings. Astrophys. J. 797, 93.

Zebker, H. A., Marouf, E. A., Tyler, G. L. 1985. Saturn's rings - Particle size distributions for thin layer model. Icarus 64, 531-548.

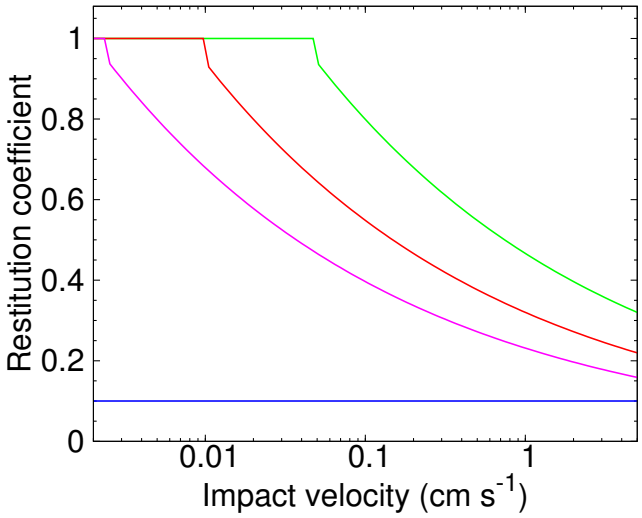

Figure 1. Four kinds of restitution coefficient laws used in the present study. (i) Constant normal restitution coefficient, $\varepsilon_{\rm n} = 0.1$ (blue); (ii) the velocity-dependent restitution coefficient based on Bridges et al. (1984) given by Eq.(2) with $v_{\rm c} = 1{\rm cm\ s}^{-1} (\equiv v_{\rm B})$ (red); (iii) the expression (2) with $v_{\rm c} = 0.25 v_{\rm B}$ (magenta); and (iv) the expression (2) with $v_{\rm c} = 5 v_{\rm B}$ (green).

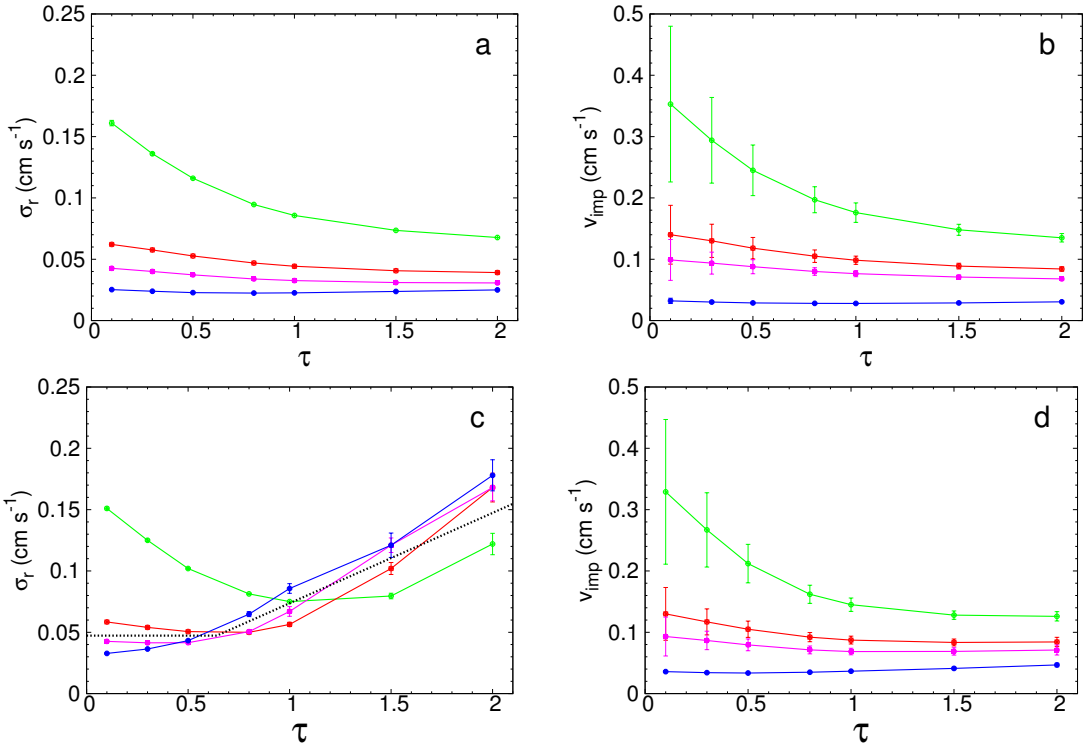

Figure 2. Radial component of velocity dispersion (panels a and c) and mean impact velocity (panels b and d) as a function of ring's optical depth. Marks represent mean values after the system reached a quasi-steady state, with error bars showing dispersions. Panels a and b show the non-gravitating case, while c and d show the self-gravitating case. The colors represent different restitution coefficient laws shown in Figure 1. The dotted line in panel c represents the semi-analytic expression $\sigma_{\rm r} = \max\{\sigma_{\rm enc}, 0.6\sigma_{\rm wake}\}$. Numbers of particles used in simulation vary from 3,000 to $\sim$ 57,000 depending on the optical depth ($R = 100$cm, $\rho = 0.4$ g cm^{-3}, $a = 1 \times 10^{10}$ cm).

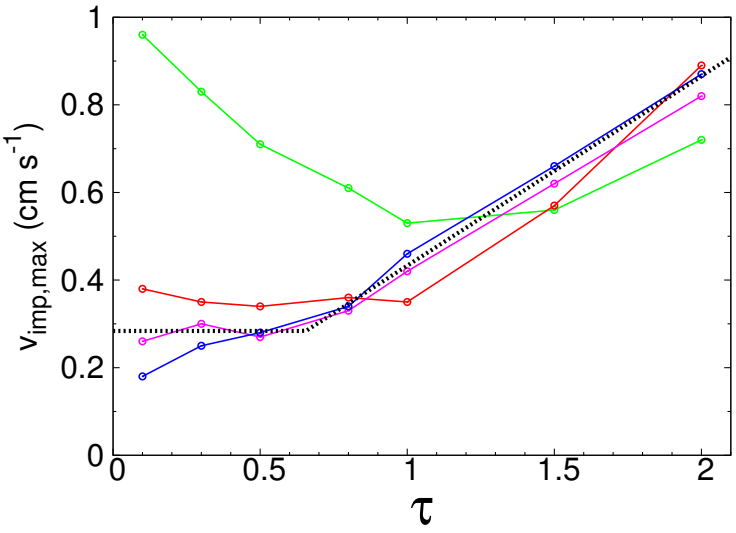

Figure 3. Maximum impact velocity as a function of the optical depth for the self-gravitating case shown in Figures 2c and 2d. The colors represent different restitution coefficient laws shown in Figure 1. The dotted line represents the semi-analytic expression $v_{\rm imp,max} = \max\{6v_{\rm esc}, 0.4\lambda_{\rm cr}\Omega\}$ (see text).

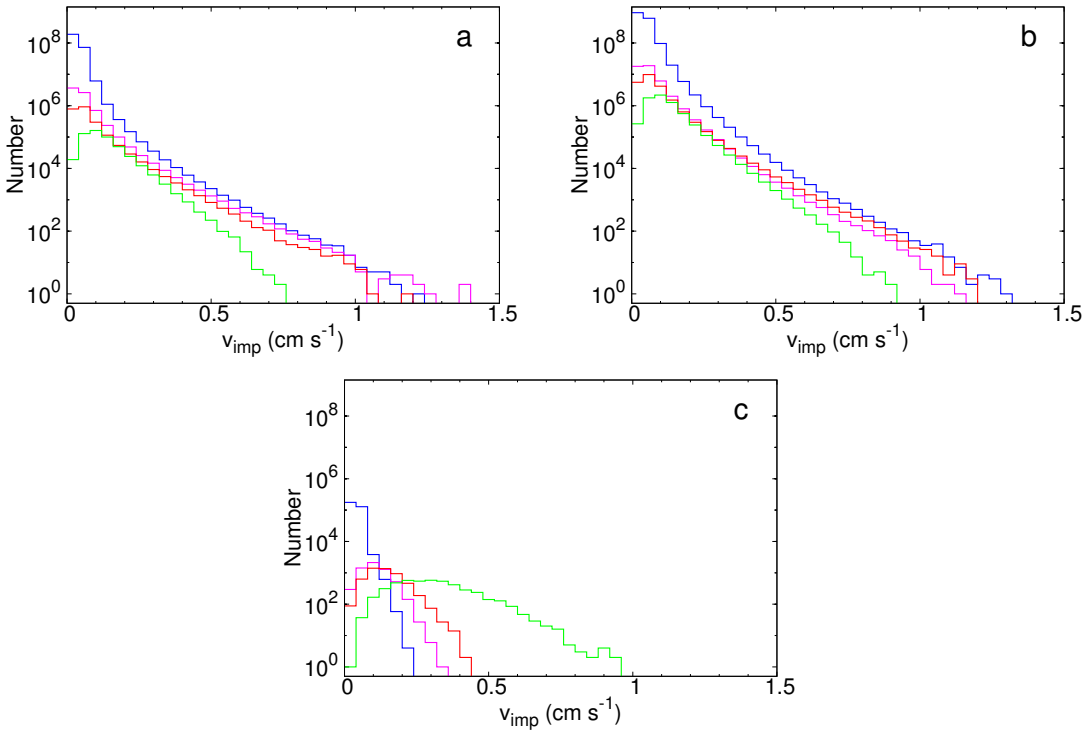

Figure 4. Distribution of impact velocities for the three cases of rings with equal-sized particles. The radial location and surface density for the cases shown in panels a, b, and c correspond to the A, B, and C rings, respectively. The colors represent different restitution coefficient laws shown in Figure 1. The values of the semi-major axis, optical depth, and r_h in these cases are: (a) $a = 1.28 \times 10^{10}$ cm, $\tau = 0.77$, and $r_h = 0.80$; (b) $a = 1.05 \times 10^{10}$ cm, $\tau = 2$, and $r_h = 0.66$; and (c) $a = 0.85 \times 10^{10}$ cm, $\tau = 0.1$, and $r_h = 0.53$, respectively Numbers of particles used in simulation are 16,000 (a), 75,000 (b), and 5,000 (c), respectively ($\rho = 0.4$ g cm^{-3}).

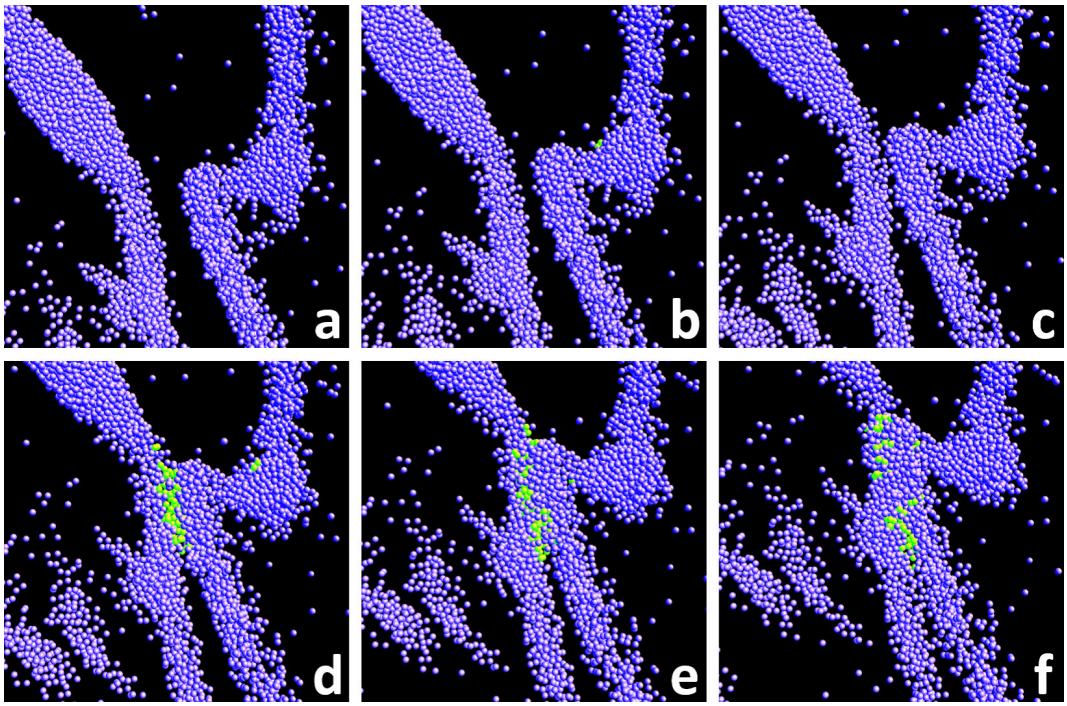

Figure 5. A series of snapshots of particle distribution showing collision between adjacent gravitational wakes causing high-velocity impacts between particles. A part of the simulation cell for the case of the A ring is shown, where $\varepsilon_{\rm n} = \varepsilon_{\rm n}(v)$ with $v_{\rm c} = v_{\rm B}$ (corresponding to the red curve in Figure 4a). Panels a to f show the time evolution of the same small region with the time interval of 0.01 $T_{\rm K}$ ($T_{\rm K}$ is the orbital period). Collision between adjacent gravitational wakes takes place in panels d to f. Those particles that experienced high-velocity impacts ($v_{\rm imp} > 0.3$ cm s^{-1}) during the last $0.002T_{\rm K}$ are shown in green.

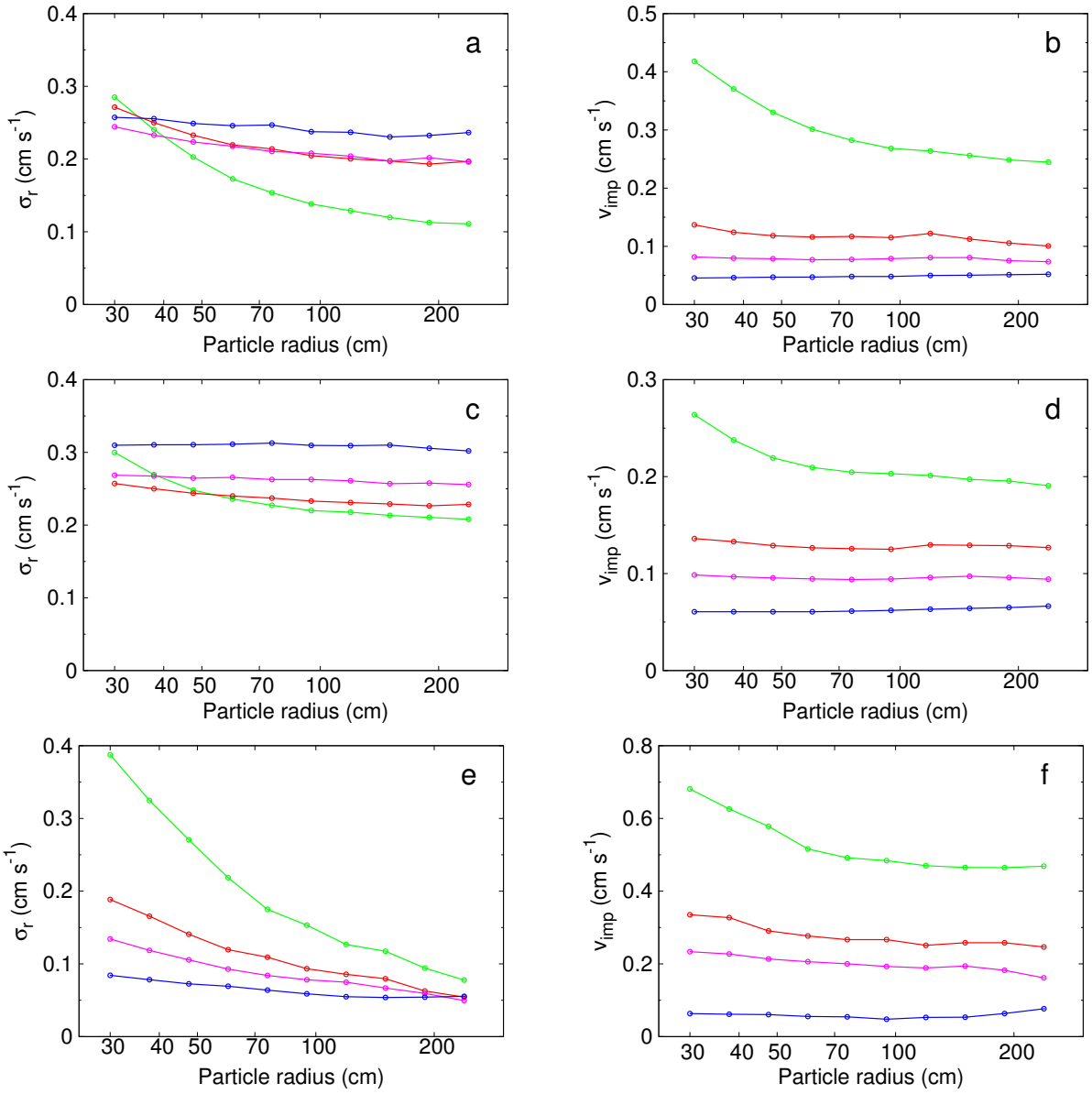

Figure 6. Radial velocity dispersion (panels a, c, and e) and mean impact velocity (panels b, d, and f) as a function of particle size in the case of particle size distribution. Panels a and b show the case of the A ring; panels c and d show the case of the B ring; and panels e and f show the case of the C ring. We assumed a power-law size distribution with $n(R)dR \propto R^{-3}dR$ for 30 cm $\leq R \leq$ 300 cm. In this case, r_h takes on the following range of values depending on the mass ratio of the colliding pairs: $0.80 \leq r_h \leq 1.16$ for the case of the A ring; $0.66 \leq r_h \leq 0.95$ for the B ring; and $0.53 \leq r_h \leq 0.77$ for the C ring, respectively. The colors represent different restitution coefficient laws shown in Figure 1. Numbers of particles used in simulation are 32,000 (a and b), 149,500 (c and d), and 11,000 (e and f), respectively ($\rho = 0.4$ g cm^{-3}).

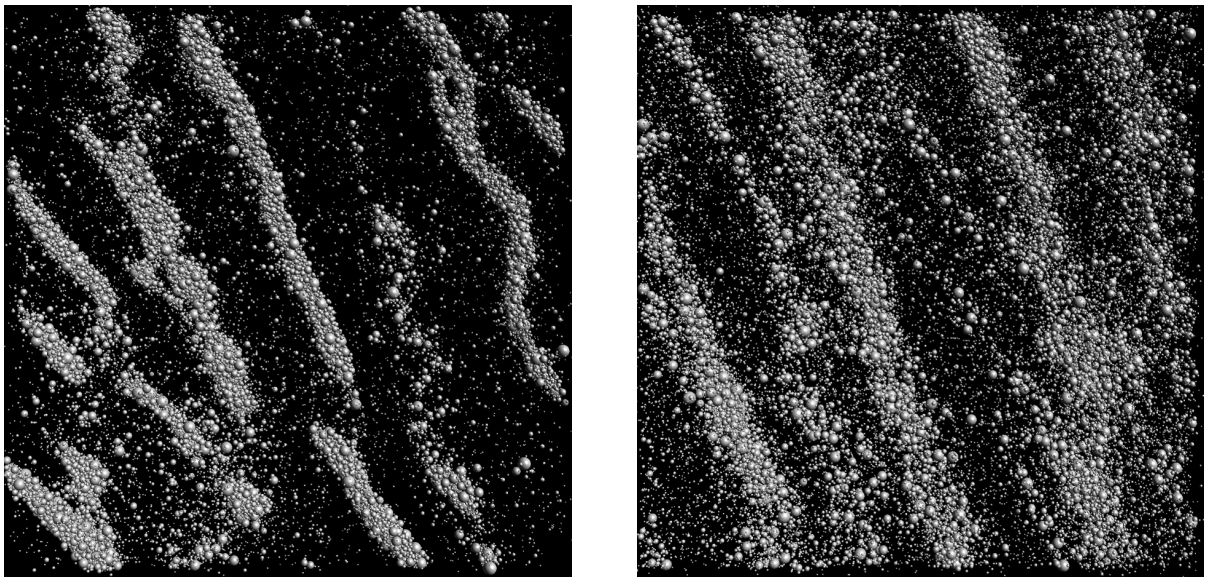

Figure 7. Snapshots for the case of the A ring with particle size distribution. The left panel shows the case of highly inelastic particles with the velocity-dependent restitution coefficient given by Eq.(2) with $v_c = 0.25 v_B$, and the right panel shows the case of more elastic particles with $v_c = 5 v_B$.

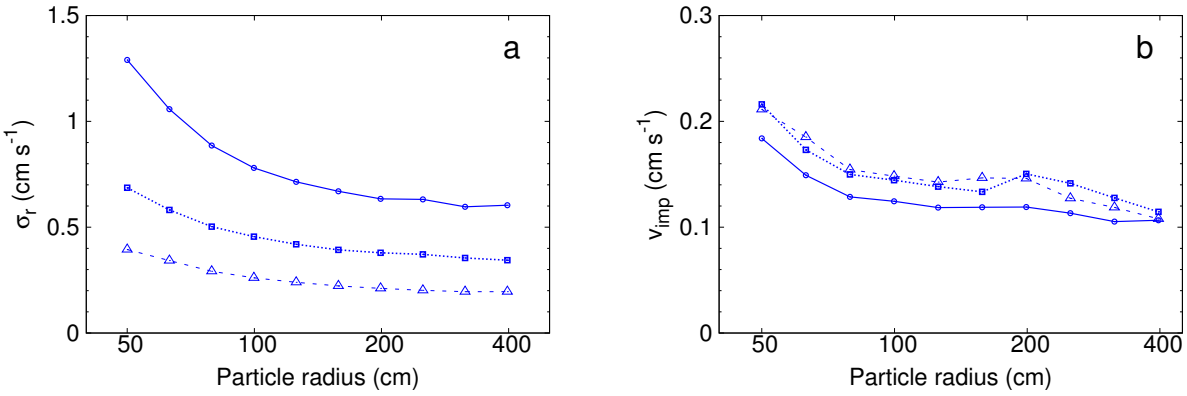

Figure 8. Dependence of the velocity dispersion and mean impact velocity on particles' material density in the case of size distribution. Cases with $\rho = 0.9$ (solid lines with circles), 0.6 (dotted lines with squares), and 0.4 g cm^{-3} (dashed lines with triangles) are shown. $a = 1.28 \times 10^{10}$cm, 50 cm $\leq R \leq$ 500 cm, and $\varepsilon_n = 0.5$.

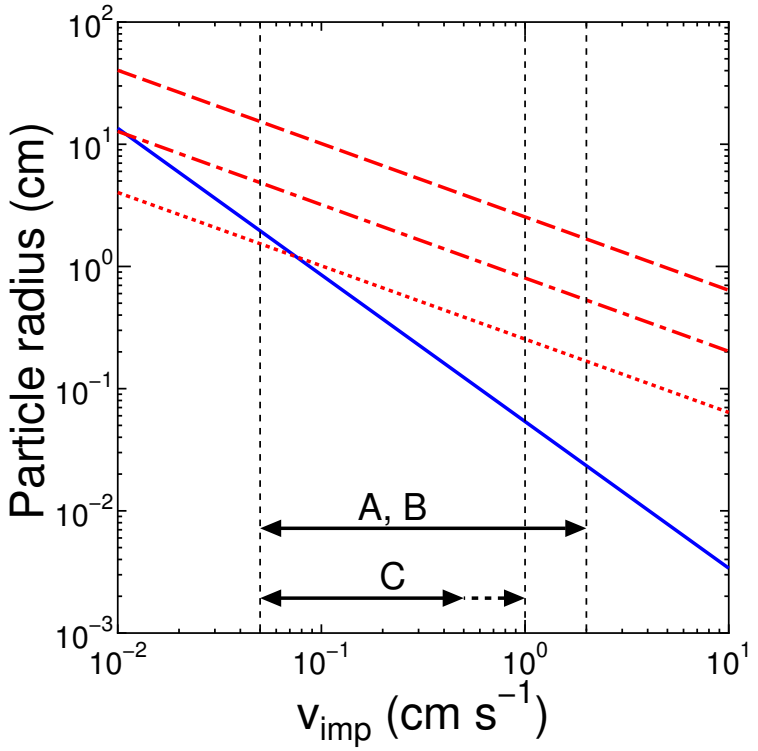

Figure 9. Critical particle radius for sticking ($R_{\rm stc}$ given by Eq.(9); solid line) and that for collisional detachment ($R_{\rm det}$ given by Eq.(10)) as a function of impact velocity. The dotted line, dot-dashed line, and dashed line represent $R_{\rm det}$ for the case of $R_{\rm L}$ = 1cm, 10 cm, and 100 cm, respectively. We assumed $\gamma = 0.38$ J m^{-2}. The approximate ranges of impact velocities obtained from the present study are also shown by the vertical dotted lines. In the case of the A and B rings, $0.05 \lesssim v_{\rm imp} \lesssim 2$ cm s^{-1}. In the case of the C ring, $0.05 \lesssim v_{\rm imp} \lesssim 0.5$ cm s^{-1} when collisions are sufficiently dissipative, while the maximum value can be larger if collisions are more elastic as in the case (iv) shown in Figure 1.